ChemComm

COMMUNICATION

View Article Online
View Journal | View Issue

Cite this: *Chem. Commun.*, 2024, **60**, 10724

Received 13th August 2024,
Accepted 28th August 2024

DOI: 10.1039/d4cc04126g

rsc.li/chemcomm

Rational design of a red-light absorbing ruthenium polypyridine complex as a photosensitizer for photodynamic therapy†

Alessia Fennes, Nicolás Montesdeoca, Zisis Papadopoulos and Johannes Karges *

Herein, the computer-guided design, chemical synthesis, and biological evaluation of a Ruc polypyridine complex, that could eradicate cancerous cells upon excitation with red light at 630 nm, is reported.

Photodynamic therapy (PDT) is a non-invasive medical technique used to treat various cancers (*i.e.*, lung, bladder, esophageal, or brain cancers) as well as bacterial, fungal, or viral infections. During PDT, a non-toxic dose of a photosensitizer is administered either locally or systemically. Initially, the photosensitizer is distributed throughout the body, but it (preferentially) accumulates in the target tissue. Following a certain incubation time, the target tissue is exposed to irradiation, triggering a therapeutic PDT effect. Notably, this effect occurs exclusively in the irradiated tissue that contains the photosensitizer.[1,2] To date, the majority of studied photosensitizers are based on a tetrapyrrolic structural scaffold (*i.e.*, porphyrin, chlorin, bacteriochlorin, or phthalocyanine), which significantly influences their photophysical and biological properties. Due to this common structural feature, many of these photosensitizers exhibit similar drawbacks, including poor water solubility, low photostability, tedious synthesis and purification, and slow clearance from the body leading to prolonged photosensitivity.[3] To overcome these limitations, there is a high demand for the modification or the development of new structural scaffolds for photosensitizers. Among the most promising classes, significant research effort has been devoted towards Ru(II) polypyridine complexes due to their attractive photophysical and biological properties (*i.e.*, strong emission, high (photo-)stability, high biocompatibility, high water solubility).[4–6] Worthy of note, the Ru(II) polypyridine complex TLD-1433 has advanced into phase II clinical trials for the treatment of bladder cancer.[7] Despite promising biological properties, the vast majority of Ru(II) polypyridine complexes are excited with ultraviolet or blue light.[8,9] As these wavelengths are poorly penetrating the cancerous tissue, these compounds could only find application towards the treatment of superficial tumors. To enable the treatment of large or deep-seated cancerous tumors, there is a need for the development of photosensitizers that could be excited in the biological spectral window (600–900 nm).[10] To overcome this limitation, herein, the computer-aided rational design, chemical synthesis, and biological evaluation of a Ru(II) polypyridine complex, that could be excited and eradicate cancerous cells as well as multicellular tumor spheroids with red light at 630 nm, is reported.

Previous studies have demonstrated, in a simplified model, that the highest occupied molecular orbitals (HOMO) in a pseudo-octahedral Ru(II) polypyridine complex are the ruthenium t_{2g} d orbitals, while the lowest unoccupied molecular orbitals (LUMO) typically are the π* orbitals localized on the ligands. Therefore, the lowest energy absorption band of this compound corresponds to a metal-to-ligand charge transfer (MLCT), resulting from electronic transitions from the t_{2g} manifold to the empty π* orbitals of the ligands.[11] A straightforward approach to shift the excitation band towards longer wavelength is to decrease the HOMO–LUMO gap through targeted functionalization of the ligand. Capitalizing on this, the conjugated π-system of the ligand scaffold of the parent complex $[Ru(2,2'\text{-bipyridine})_3]^{2+}$ was systemically extended and the respective energies calculated by (time-dependent) density functional theory (TD-DFT) calculations. While the functionalization with the allyl-group showed only a small difference in the HOMO–LUMO gap to the parent complex, the modification of the ligand scaffold with bisstryl-groups strongly reduced the HOMO–LUMO gap (2.30 eV). Notably, previous studies have demonstrated the potential of (*E*,*E*′)-4,4′-bisstyryl-2,2′-bipyridine coordinated Ru(II) polypyridine complexes for PDT.[12,13] Further exploration of the modification of the ligand scaffold demonstrated that the HOMO–LUMO could be additionally reduced upon functionalization with diphenylamino groups (1.91 eV) (structure of proposed compounds: Fig. 1(A), coordinates of

Faculty of Chemistry and Biochemistry, Ruhr-University Bochum, Universitätsstrasse 150, 44780 Bochum, Germany. E-mail: johannes.karges@ruhr-uni-bochum.de; Web: https://www.kargesgroup.ruhr-uni-bochum.de; Tel: +49 2343224187

† Electronic supplementary information (ESI) available. See DOI: https://doi.org/10.1039/d4cc04126g

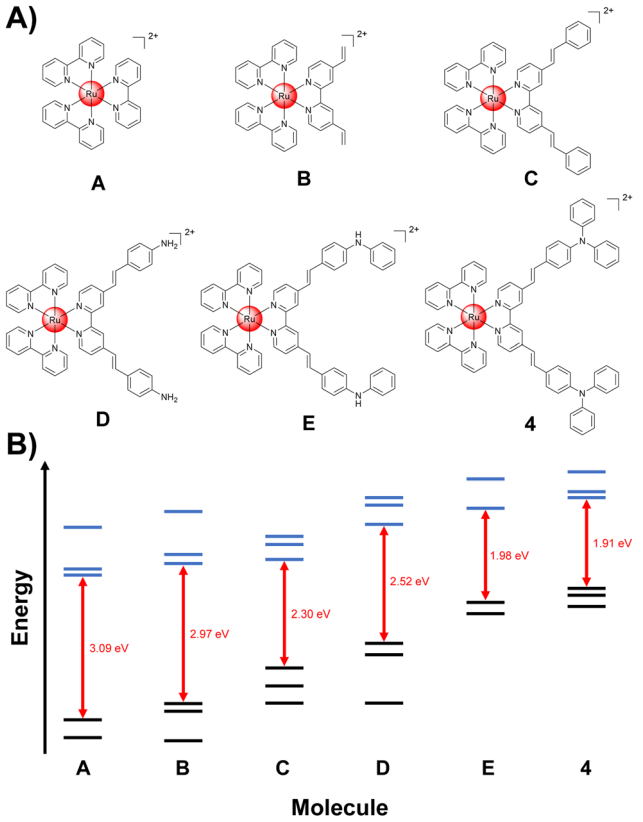

Fig. 1 DFT-guided rational design of Ru(II) polypyridine complexes with absorption at longer wavelengths. (A) Proposed structures of metal complexes. (B) Computed frontier orbital energies and HOMO–LUMO gaps of proposed structures. Occupied orbitals are represented as black lines and unoccupied orbitals are represented as blue lines. The HOMO–LUMO gap is represented as a red arrow.

structures proposed compounds: Tables S1–S6 (ESI†), calculated energy levels: Fig. 1(B)). Additional analyses have shown that the lowest energy band in the computationally optimized metal complex, followingly referred to as **4**, is attributed to MLCT transition of the ruthenium t_{2g} manifold to the empty π^* orbitals of the ligands (Fig. S1, ESI†).

Based on this theoretical insight, the chemical synthesis of the computationally optimized metal complex **4** was attempted. Ru(III)–chloride was reduced with ethanol to Ru(II) and the coordination sphere was saturated with dimethyl sulfoxide ligands to form compound **1**. The synthesized metal precursor was subsequently heated under reflux in *N*,*N*-dimethylformamide with two equivalents of 2,2′-bipyridine in the presence of an excess of lithium chloride. The product [Ru(2,2′-bipyridine)$_2$(Cl)$_2$] **2** was isolated by precipitation through the addition of acetone. The π-extended ligand (*E*,*E*′)-4,4′-bis[*p*-(*N*,*N*-phenylamino)styryl]-2,2′-bipyridine **3** was synthesized upon mixing of 4,4-dimethyl-2,2′-bipyridine and 4-(diphenylamino)benzaldehyde in dry *N*,*N*-dimethylformamide in the presence of potassium *tert*-butoxide under argon atmosphere. The compound was isolated upon precipitation out of water and recrystallization from acetic acid. The desired Ru(II) polypyridine complex [Ru(2,2′-bipyridine)$_2$((*E*,*E*′)-4,4′-bis[*p*-(*N*,*N*-phenyl-amino)-styryl]-2,2′-bipyridine)] **4** was prepared upon refluxing of **2** and **3**

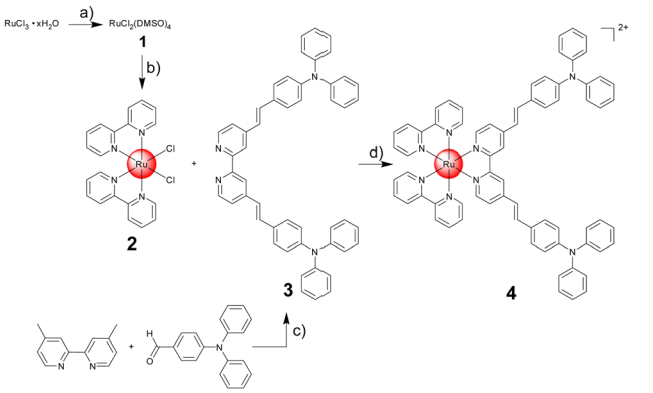

Fig. 2 Synthesis of the desired Ru(II) polypyridine complex **4**. (a) 1. ethanol, reflux, 3 h; 2. dimethyl sulfoxide, 150 °C, 2 h; (b) 2,2′-bipyridine, lithium chloride, dry *N*,*N*-dimethylformamide, reflux, 4 h; (c) potassium *tert*-butoxide, dry *N*,*N*-dimethylformamide, room temperature, 24 h; (d) ethanol, reflux, 24 h. The metal complex was isolated as a hexafluorophosphate salt.

in dry ethanol overnight. The metal complex was isolated by silica column chromatography and precipitation from ammonium hexafluorophosphate (Fig. 2). All compounds were characterized by NMR spectroscopy and mass spectrometry (Fig. S2–S11, ESI†). The purity of the lead complex was verified by elemental analysis.

With the compound in hand, the photophysical properties of **4** were studied in water. The metal complex had an intense absorption peak of the ligand-centered transition at 290 nm (ε = 123.7 × 10^3 M^{-1} cm^{-1}) as well as the metal-to-ligand charge transfer transitions centered at 439 nm (ε = 65.9 × 10^3 M^{-1} cm^{-1}) and 494 nm (ε = 56.7 × 10^3 M^{-1} cm^{-1}) (absorption spectrum: Fig. 3, extinction coefficients: Table S7, ESI†). In agreement with the theoretical prediction, the metal complex showed an absorption in the red region of the spectrum as well as an absorption tail in the near-infrared region (630 nm, ε = 457 M^{-1} cm^{-1}). Notably, previous studies have shown that photosensitizers could be active despite having excitation coefficients below 100 M^{-1} cm^{-1}.[14] Upon excitation at 420 nm, the metal complex emitted light centered at 692 nm (emission spectrum: Fig. S12, ESI†). The direct comparison of **4** and the parent complex [Ru(2,2′-bipyridine)$_3$][Cl]$_2$ demonstrated a similar emission quantum yield (**4**: 3.8%; [Ru(2,2′-bipyridine)$_3$][Cl]$_2$: 4.0%). The ability to catalytically convert molecular oxygen into singlet oxygen was measured using the singlet oxygen probe 1,3-diphenylisobenzofuran. Generated singlet oxygen can react with 1,3-diphenylisobenzofuran in a cycloaddition reaction, resulting in the quenching of its absorption peaks.

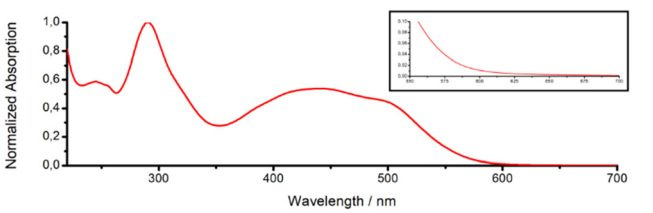

Fig. 3 Absorption spectrum of 4 in water. Inlet: magnification of the absorption in the red region.

Time-dependent monitoring of this peak allows for the estimation of the catalytic singlet oxygen production. The direct comparison showed that **4** had a 1.4-times stronger singlet oxygen production than the parent complex $[Ru(2,2'\text{-bipyridine})_3][Cl]_2$ (Fig. S13, ESI†).

The stability of a compound in an aqueous solution is of crucial importance for any potential biological application. To investigate the stability of the metal complex, **4** was dissolved in water or DMEM cell media and the absorption spectrum was measured after 48 h. As no significant changes were observed, the stability under aqueous conditions is indicated (Fig. S14 and S15, ESI†). Followingly, the photostability of the metal complex was studied upon constant irradiation for 60 min in water. Upon irradiation over longer times, slight changes in the absorption spectra were observed, that could indicate for instabilities upon light exposure (Fig. S16, ESI†). In direct comparison under identical conditions, the parent compound $[Ru(2,2'\text{-bipyridine})_3][Cl]_2$ (Fig. S17, ESI†) did not show any changes in the absorption profile and the photosensitizer Photofrin (Fig. S18, ESI†) demonstrated a loss in the signal intensity. For a deeper insight into the photostability, the metal complex was irradiated for 60 min and the identity of the compound analyzed by NMR spectroscopy. The spectra showed that the metal complex remained intact with some minor peaks emerging, that could explain the changes in the absorption spectra (Fig. S19, ESI†).

The lipophilicity of the Ru(II) polypyridine complex was assessed by determining the distribution coefficient ($\log P$) between the phosphate-buffered saline and octanol phases using the shake-flask method. The metal complex **4** was present in the phosphate-buffered saline and octanol phases, indicating a balanced lipophilic and hydrophilic nature ($\log P = +0.6 \pm 0.1$), which is considered ideal for a drug candidate. The cell membrane permeability was simulated using a parallel artificial membrane permeability assay. The metal complex **4** demonstrated a high permeability rate (0.042 ± 0.003 μm s^{-1}) when compared to well-characterized control compounds with known permeability rates (Table S8, ESI†).

Based on these promising photophysical and pharmacological properties, the therapeutic effect of **4** was evaluated in comparison to the clinically applied photosensitizer Photofrin and the chemotherapeutic drug cisplatin against cancerous mouse colon carcinoma (CT-26), human breast adenocarcinoma (MCF-7), human pancreatic adenocarcinoma (PT-45), and non-cancerous human fibroblast (GM-5657) cells. The cells were incubated with the compounds for 4 h, washed to remove any non-internalized compound, irradiated with blue (450 nm, power: 20%, 10 min, 1.2 J cm^{-2}) or red light (630 nm, power: 10%, 15 min, 0.9 J cm^{-2}), and after an additional 44 h the cell viability was assessed using the dye 3-(4,5-dimethylthiazol-2-yl)-2,5-diphenyltetrazolium bromide (MTT). Importantly, the Ru(II) polypyridine complex **4** was found to be non-toxic against all investigated cell lines. This is a crucial requirement for a PDT agent. Contrary, the metal complex induced a phototoxic effect in the very low micromolar range upon irradiation with blue or red light. Among the investigated cell lines, **4** caused the strong therapeutic response against CT-26 cells ($IC_{50,dark} > 100$ μM, $IC_{50,450nm} = 0.8 \pm 0.1$ μM, $IC_{50,630nm} = 1.3 \pm 0.2$ μM), corresponding to phototoxic indices of >125 for the blue light irradiation and >77 for the red-light irradiation. Based on these findings, further experiments were performed in CT-26 cells. Promisingly, **4** was found to be significantly stronger therapeutically active than the clinically applied photosensitizer Photofrin (Table 1).

For a deeper understanding of the observed phototoxic effect, the ability of **4** to generate reactive oxygen species upon irradiation was studied by using fluorescence microscopy using the reactive oxygen species-specific probe 2′,7′-dichlorodihydrofluorescein diacetate. While this dye is non-fluorescent in human cells, it gets readily oxidized by reactive oxygen species into a highly green-fluorescent molecule. The microscopy images of the cancer cells treated with **4** in the dark showed no green fluorescence, indicating no or only little amount of reactive oxygen species. In contrast, strong green fluorescence was observed in cancer cells treated with complex **4** and exposure to red light (Fig. 4), suggesting its effective reactive oxygen species generation properties inside the cancer cells.

Based on the strong therapeutic response against two-dimensional cancer monolayer cells, the biological effects against three-dimensional multicellular tumor spheroids were studied. Multicellular tumor spheroids are a tissue culture model that mimics pathological conditions of clinical tumors such as proliferation and nutrient gradients or a hypoxic center. Herein, multicellular tumor spheroids with an average diameter of approximately 600 μm were grown and used to study the therapeutic efficiency of the metal complex using a commercial CellTiter-Glo 3D Cell Viability kit. While **4** was found to be non-toxic in dark, the Ru(II) polypyridine complex generated a therapeutic effect in the low micromolar range upon irradiation with red light ($IC_{50,dark} > 100$ μM, $IC_{50,630nm} = 8.4 \pm 0.6$ μM). For a

Table 1 IC_{50} values in μM of the Ru(II) polypyridine complex 4 in comparison to the clinically applied photosensitizer Photofrin and the chemotherapeutic drug cisplatin in mouse colon carcinoma (CT-26), human breast adenocarcinoma (MCF-7), human pancreatic adenocarcinoma (PT-45), and non-cancerous human fibroblast (GM-5657) cells in the dark or upon blue (450 nm, power: 20%, 10 min, 1.2 J cm^{-2}) or red (630 nm, power: 10%, 15 min, 0.9 J cm^{-2}) light irradiation. Three independent measurements as mean ± standard deviation

	CT-26			MCF-7			PT-45			GM-5657		
	Dark	450 nm	630 nm	Dark	450 nm	630 nm	Dark	450 nm	630 nm	Dark	450 nm	630 nm
4	>100	0.8 ± 0.1	1.3 ± 0.2	>100	2.4 ± 0.2	6.4 ± 0.3	>100	1.6 ± 0.1	2.7 ± 0.3	>100	3.3 ± 0.4	5.4 ± 0.3
Photofrin	>50[a]	4.1 ± 0.6	2.4 ± 0.5	>50[a]	3.6 ± 0.3	2.9 ± 0.3	>50[a]	9.7 ± 1.1	7.4 ± 0.6	>50[a]	4.8 ± 0.5	3.9 ± 0.4
Cisplatin	6.3 ± 0.5	—	—	8.1 ± 0.6	—	—	11.3 ± 0.4	—	—	9.3 ± 0.6	—	—

[a] Maximal solubility of Photofrin within cell media.

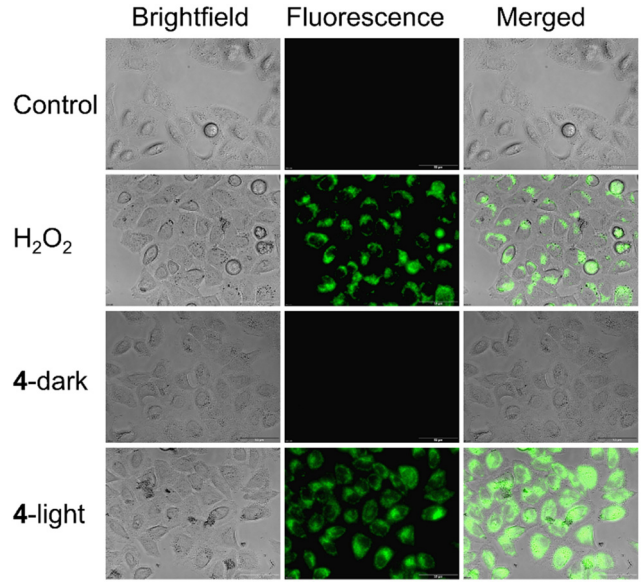

Fig. 4 Fluorescence microscopy images of CT-26 upon treatment with **4** (1.3 μM) in the dark or exposure to red light (630 nm, power: 10%, 7.5 min, 0.45 J cm^{-2}) or hydrogen peroxide as a positive control. Scale bar = 50 μm.

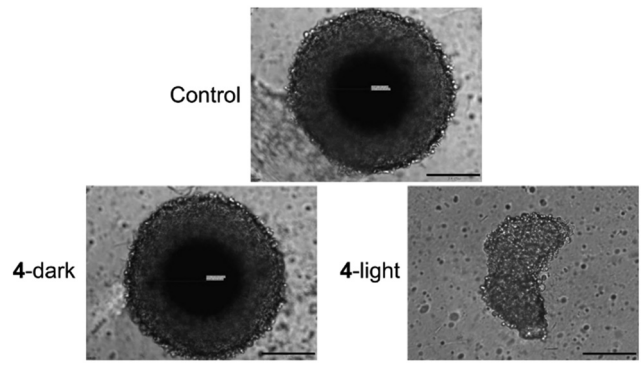

Fig. 5 Light microscopy images of CT-26 multicellular tumor spheroids upon treatment with 4 (20 μM) in the dark or exposure to red light (630 nm, power: 10%, 15 min, 0.9 J cm^{-2}). Scale bar = 200 μm.

deeper understanding of the therapeutic effects, the size and morphology of the treated multicellular tumor spheroids were analyzed by light microscopy. The treatment with **4** in the dark did not affect the size or morphology of the tumor spheroids. In contrast, treatment with compound **4** and exposure to red light led to a drastic reduction in tumor size and strong morphological damage (Fig. 5), highlighting its ability to act as a photosensitizer for PDT.

In summary, this study reports on the computer-guided design, chemical synthesis, and biological evaluation of a Ru(II) polypyridine complex for PDT. The lead compound was designed to be excited with a red light at 630 nm, allowing for potential deep tissue penetration and therefore the treatment of deep-seated tumors. Strikingly, the compound demonstrated a stronger therapeutic response than the clinically applied photosensitizer Photofrin. We are confident that this study will open new avenues for the treatment of large or deep tumors.

J. Karges gratefully acknowledges the financial support provided by the Liebig fellowship from the Chemical Industry Fund of the German Chemical Industry Association, the Life Sciences Bridge Award from the Aventis Foundation, and the Paul Ehrlich & Ludwig Darmstaedter Early Career Award 2024 – a prize awarded by the Paul Ehrlich Foundation, Germany.

Data availability

The data supporting the findings of this study are available within the article and its ESI.†

Conflicts of interest

There are no conflicts to declare.

References

1 S. Callaghan and M. O. Senge, *Photochem. Photobiol. Sci.*, 2018, **17**, 1490–1514.
2 J. Karges, *Angew. Chem., Int. Ed.*, 2022, **61**, e202112236.
3 A. E. O'Connor, W. M. Gallagher and A. T. Byrne, *Photochem. Photobiol.*, 2009, **85**, 1053–1074.
4 S. Bonnet, *J. Am. Chem. Soc.*, 2023, **145**, 23397–23415.
5 D. Havrylyuk, A. C. Hachey, A. Fenton, D. K. Heidary and E. C. Glazer, *Nat. Commun.*, 2022, **13**, 3636.
6 X. Zhao, J. Liu, J. Fan, H. Chao and X. Peng, *Chem. Soc. Rev.*, 2021, **50**, 4185–4219.
7 S. Monro, K. L. Colón, H. Yin, J. Roque, III, P. Konda, S. Gujar, R. P. Thummel, L. Lilge, C. G. Cameron and S. A. McFarland, *Chem. Rev.*, 2019, **119**, 797–828.
8 J. Liu, C. Zhang, T. W. Rees, L. Ke, L. Ji and H. Chao, *Coord. Chem. Rev.*, 2018, **363**, 17–28.
9 M. Ankathatti Munegowda, A. Manalac, M. Weersink, S. A. McFarland and L. Lilge, *Coord. Chem. Rev.*, 2022, **470**, 214712.
10 K. Ogawa and Y. Kobuke, *Anti-Cancer Agents Med. Chem.*, 2008, **8**, 269–279.
11 S. Campagna, F. Puntoriero, F. Nastasi, G. Bergamini and V. Balzani, in *Photochemistry and Photophysics of Coordination Compounds I*, ed. V. Balzani and S. Campagna, Springer Berlin Heidelberg, Berlin, Heidelberg, 2007, pp. 117–214.
12 J. Karges, S. Kuang, F. Maschietto, O. Blacque, I. Ciofini, H. Chao and G. Gasser, *Nat. Commun.*, 2020, **11**, 3262.
13 J. Karges, S. Kuang, Y. C. Ong, H. Chao and G. Gasser, *Chem. – Eur. J.*, 2021, **27**, 362–370.
14 H. Yin, M. Stephenson, J. Gibson, E. Sampson, G. Shi, T. Sainuddin, S. Monro and S. A. McFarland, *Inorg. Chem.*, 2014, **53**, 4548–4559.